UNIVERSITÀ DEGLI STUDI DI PADOVA

UNIVERSITA' DEGLI STUDI DI PADOVA

Dipartimento di Ingegneria Industriale DII

Dipartimento di Fisica e Astronomia "Galileo Galilei"

Corso di Laurea in Ingegneria Aerospaziale

Evaluating the flux of cosmic protons along the orbit of a Compton gamma-ray space telescope

Relatore: Riccardo Rando

Riccardo Dal Moro 1069920

Anno Accademico 2017/2018

Contents

List of Figures

Preface

Content of the thesis

The purpose of this work is to derive the required data for the design of a nano satellite for MeV gamma-ray astrophysics by the University of Padova.

The main concern is to describe the flux of trapped and primary protons along a near equatorial orbit. This is of interest since protons can activate spacecraft's materials and therefore cause a significant instrumental background.

Chapter 1

Introduction

1.1 Gamma ray observation

Gamma ray astronomy is a brand of astrophysics based on the observation of gamma ray emission from the Universe.
There are different possible sources, the MeV range rays are produced by the solar activity but the higher range (GeV) is produced only by extra solar system phenomena.
Recent missions of interest are: SWIFT (NASA, 2004) for the detection of Gamma ray bursts, Beppo-Sax (Italy and Netherlands, 1996) for the study of Gamma ray bursts in the X-ray range, INTEGRAL (INTernational Astrophysics Gamma Ray, ESA, 2002), FERMI (NASA and other agencies, 2008) and AGILE (Astrorivelatore Gamma ad Immagini Leggero, Italy, ASI, INFN, INAF, 2007)

For the study of this kind of radiation we use satellites in orbit to bypass the shield of the atmosphere. This expose spacecraft to radiations that can damage the instruments and affect the measurements of the extra-solar rays. In quasi-equatorial low Earth orbit the highest amount of radiation is in the form of protons, both primary and trapped inside the magnetosphere.

1.2 Earth's atmosphere

The atmosphere is a continuous medium formed by different layers of gases that cover the Earth. It can be represented schematically as 5 principal layers:

Exosphere: from 700 to 10000 km, is the higher layer and it is formed by low density helium and hydrogen and particles that are moving in and out the magnetosphere and from the solar winds.
Thermosphere: from 80 to 700 km
Mesosphere: from 50 to 80 km
Stratosphere: from 12 to 50 km
Troposphere: from 0 to 12 km, is the lower layer of the atmosphere. The troposphere contains 80% of the total atmospheric mass and more than the 50% of it is located inside the first 6 km.

E.g: a Low Earth Orbit (LEO) at 550 km of altitude travels inside the Thermosphere and due to the low density of the gases we can neglect the aerodynamic interactions between a spacecraft and the environment.

1.3 Earth's magnetic field and magnetosphere

The planet produces internally a magnetic field that interacts with the solar wind. The region of space around the planet where the motion of the particles is dominated by the magnetic field is called "Magnetosphere".

The solar wind moves with a supersonic flow and when this flow meets the Earth's magnetic field it forms a shock wave. This wave converts part of the particle energy in thermal energy, the flow after the passage into the shock wave becomes subsonic and flows around the Earth producing a geomagnetic tail.
In Figure 1.1 we can see an idealized magnetosphere. The picture is not a static one. Since the structure of the magnetosphere is strongly affected by the solar wind there is an eleven year cycle connected with the solar activity. In addition the geomagnetic field shows a secular evolution with a decrease of circa 6% per century.

1.3.1 The IGRF models

A useful tool to describe the geomagnetic field comes from the International Association of Geomagnetism and Aeronomy (IAGA) with the International Geomagnetic

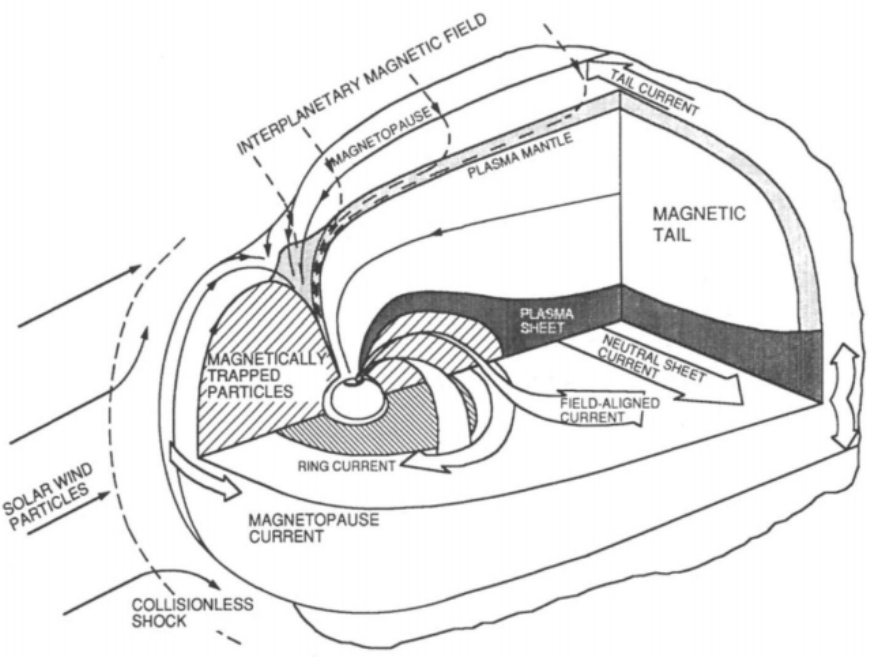

Figure 1.1: Magnetosphere's idealized representation around the Earth, from [1]

Reference Field (IGRF) mathematical models. [2].

These models provide an accurate description of the magnetic field as a multipole expansion and are valid for five years, after which they will be updated with all the correction of previous five years. In Figure 1.2 there is an example of a magnetic field map made by 2015 IGRF models.
Solar activity is not the only cause of variability affecting the magnetosphere. The magnetic field itself is not constant in time, and shows both short-term and secular variations.

1.4 Sources of radiations

The solar wind is a plasma formed by electrons, protons and alpha particles ejected from the Sun mostly due to the high energy provide by the temperature of Sun's Corona.

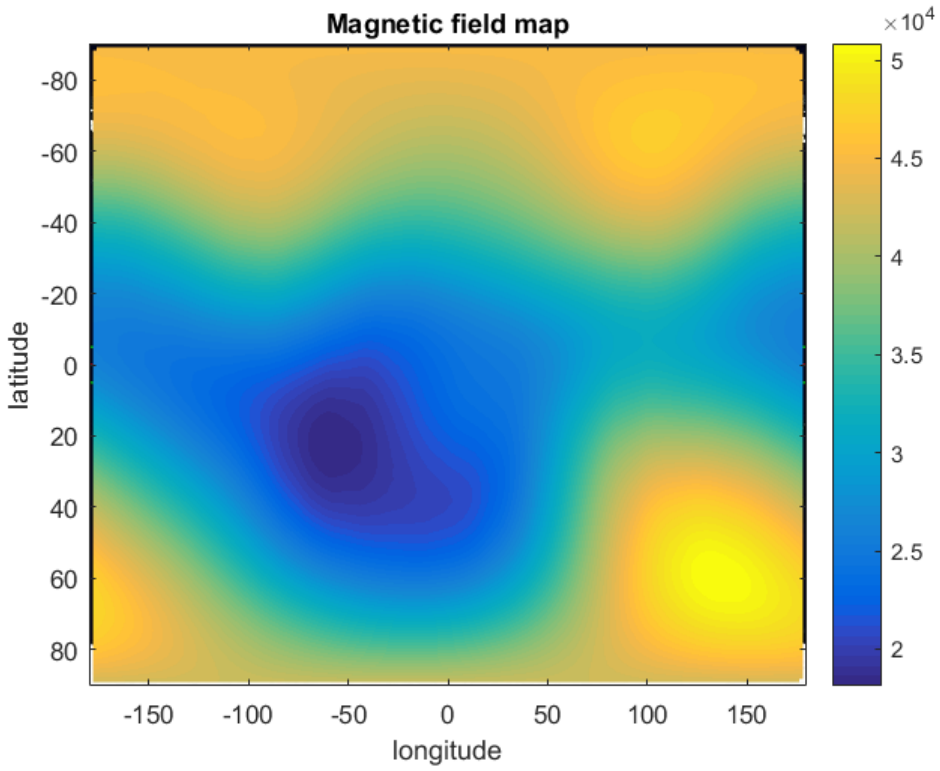

Figure 1.2: Example the average geomagnetic field intensity map at 550km of altitude as described by the 2015 IGRF model for 2019

This stream of charged particles flows from the Sun through the Solar System with a supersonic flow having a speed which is higher than all the escapes velocities of the planets (the highest escape velocity is Jupiter's, 59.54 km/sec, to be compared with the solar wind velocity that varying from 200 to 900 km/sec), this high velocity allows the particles to have a rectilinear trajectory that is not affected by gravity wells.

When the solar wind flows around the Earth a part of the stream (energetic ions and electrons) is trapped in the magnetosphere. The accumulation gives origin to radiation belts (also known as Van Allen Belts) where the trapped particles lie.

The radiation belts are a reservoir of energy that is released into the atmosphere. The result of this energy exchange is the production of phenomena like transient auroras, air-glows and the ionization of the atmosphere particles. The trapped ra-

diations, formed by charge particles, and the electric currents between the particles contribute to the local magnetic field.

1.4.1 The L-shell parameter

The most straightforward way to describe the population of the particles inside the geomagnetic field is by introducing a certain amount of adiabatic integrals, as described in [1]. For the level of detail that we need it is sufficient to reduce the complexity of the system and use a set of parameters proposed by McIlwain. The L-shell parameter (in short L) based on the value of the magnetic field B and on adiabatic invariants I:

$$LR_e = f(I, B, m_e)$$

where:

R_e is the Earth's radius,
I is the second adiabatic invariant (momentum along the field line),
B is the value of the magnetic field along the field line,
m_e is the value of the Earth's magnetic dipole,
f is a function describing an ideal dipole.

This way L indicates the maximum distance of a field line having the same magnetic proprieties as the one we are considering under the assumption of an ideal dipole.

1.4.2 Geomagnetic cut-off rigidities

Geomagnetic rigidities are a measure of the shielding effect of the Earth's magnetic field for charged particles coming from outside. With this parameter we can predict the transmission of charged particles inside the magnetosphere as a function of their rigidities. Particles below the cut-off rigidity for a given location cannot overcome the magneto-spheric shield and reach that point.

The cut-off rigidities can be calculated tracking the particle trajectory inside the magnetosphere. This process has a very high computational cost. As an approximation we can derive the L-parameter e.g from the IGRF model and than compute the

cut-off rigidities (in GV) as [3]:

$$GV = \frac{14.823}{L^{2.0311}}$$

For primaries particles the effect of the geomagnetic field is a low-energy cut-off as given above [4].

1.4.3 South Atlantic Anomaly

The South Atlantic Anomaly (SAA) is an area situated above South America and the Atlantic Ocean where the magnetic field is relatively low due to the irregularity of the Earth's dipole (see Figure 1.2).
In this region the inner radiation belts come closest to the Earth's surface causing an increased flux of energetic particles that exposes the satellites to local high levels of trapped radiations.

The SAA is growing and since his discovery (1958) the northern border is drifting eastwards but the southern is remaining in a constant position. The spot with the highest intensity is moving inside the SAA drifting westward with a speed of 0.3 degrees per year; this drift rate is similar to the differential rotation between the Earth's surface and its core. Some theories relate the drifting of the SAA and the beginning of a geomagnetic reversal [5].

1.4.4 The AP9/AE9 models

AP8 and AE8 [6] are the current version of popular empiric models describing the population of protons and electrons, respectively, around the Earth.
Currently a huge effort is undergoing to improve these models, released in 1983 (AP8) and 1976 (AE8), leading to the development of the AP9 and AE9 models, having better coverage than the previous version.

In particular AP8/AE8 models can not describe with a sufficient precision critical regions like the lowest layers of the SAA, especially in quasi-equatorial orbits.
For example in Figure 1.3 we show the average proton spectrum that a spacecraft will experience in the SAA for a quasi-equatorial orbit of 550 km of altitude with the new AP9 being developed (red) versus AP8 (green). AP8/AE8 are still recommended for

the modeling of the radiation environment but for our kind of orbit we preferred to use AP9 to get a better precision and reliability.

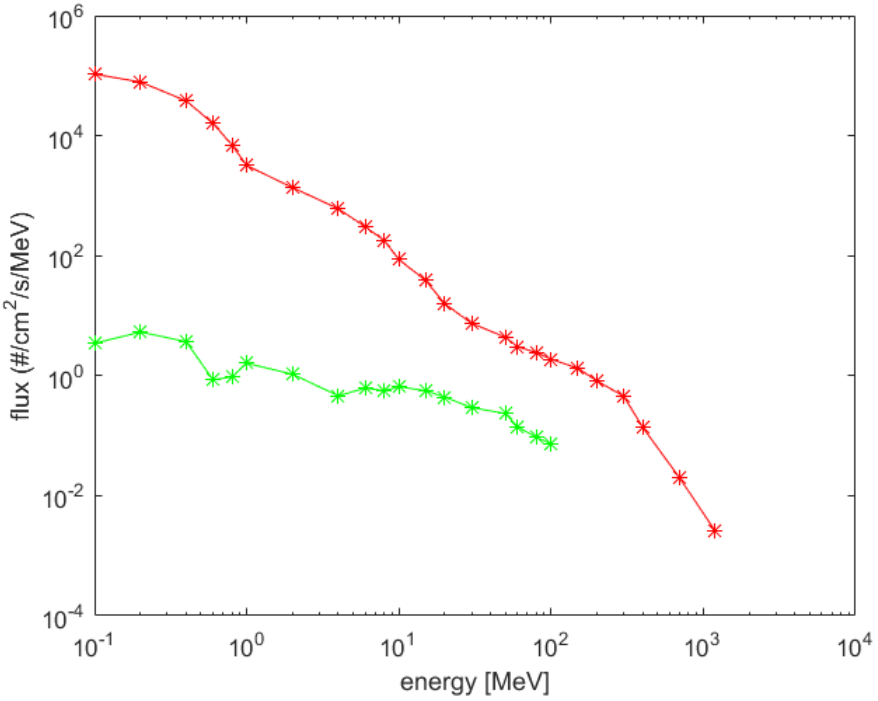

Figure 1.3: Example of the difference between AP8 (green) and AP9 (red) in SAA for a quasi-equatorial orbit at 550 km

1.5 Effects of radiation on satellite's systems

The interaction with the radiation and plasma environment is very critical for the electronic systems but also for the structural materials, solars arrays, communications, tools and battery packs.

Surface degradation

The energetic particles hit the spacecraft's surface and react causing a degradation of the thermo-optical proprieties of the materials (burnishing). The changes in the thermo-optical proprieties will affect the coefficients (absorption, reflection and transmission) that determine the thermal exchange for irradiation.

In addition, damage to the surface of the solar arrays cause a decrease in the electrical power provided to the payload.

Charge deposition

The charged particles generate a differential charge distribution and in some case this distribution causes an arc discharge (usually in the solar arrays) that could damage the local thermo-optical proprieties. If the arc is important (it uses the energy provided by the power systems) it can burn the electrical components.

Microelectronic failure

Due to miniaturization the electronic components became more sensitive to radiation damage. After a single ionizing particle hits the microelectronics the deposited charge can be sufficient to cause a flip of bi-stable memory elements changing from 0 to 1 or vice versa (Single Event Upset, the content is corrupted but the memory element is still functional).

In addition the ionizing radiation can cause a conductive paths between power elements possibly causing a permanent damage (single event latch up, single event burnout)

Total ionizing dose effects

The Total Ionizing Dose Effects (TID) are due to the accumulation of deposited charge inside the insulators. This affects the performance of microelectronic elements, e.g. CMOS transistors.

Material activation and instrumental background

Hadronic interactions in the materials can cause production of radioisotopes, with consequent emission of decay products at all time scales, from ms to years.
This is particularly relevant in the case of MeV detectors, since nuclear decay lines lie in the MeV energy band, thus causing an instrumental background.
Quantifying this is of the utmost importance for a MeV Compton telescope, see [7] for a work using preliminary results from this thesis.

Chapter 2

Thesis work

2.1 Selecting the orbit

As we had seen in 1.1 the gamma-ray observers fly in an orbit where radiation levels are the lowest possible. To avoid the SAA core we use an equatorial LEO (550 km of altitude and 5 degrees of inclination corresponding to a launch from the French Guiana). We considered an orbit starting in 2019.01.01 and a duration of 60 days, this corresponds to a condition of solar minimum.

We set the ephemerids generator to a resolution of 60 seconds and the reference system to be classical coordinates (altitude, longitude and latitude).

2.2 Magnetic field and fluxes profile inside the SAA

2.2.1 Magnetic field

First we computed the geomagnetic field along the interested orbits: with the ephemerids obtained from the AP9 suite we evaluate the magnitude of the field in every point according with the IGRF 2015 model.
The results are plotted in Figure 2.1 and as we expected over the south Atlantic area there is a depression of the field whit a minimum magnitude of $1.97 \cdot 10^4$ nT and a maximum outside the SAA about $3.35 \cdot 10^4$ nT .

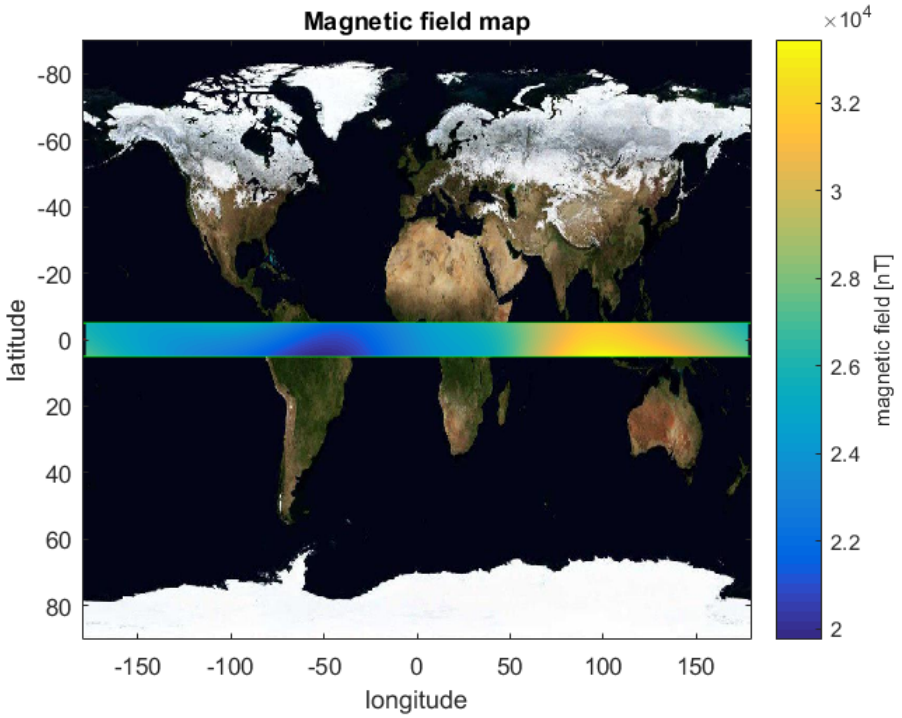

Figure 2.1: Magnetic field as a function of latitude and longitude along our orbit

2.2.2 L parameter along the orbit

Given the geomagnetic coordinates we derive the McIllwain L parameter, the results are plotted in Figure 2.2

We obtained a range of L-value that varies from 0.9847 to 1.2440.

2.2.3 Vertical cut-off

Primary protons are stopped by the magnetosphere at different energy levels. In Figure 2.3 is shown an histogram with the distribution of the geomagnetic cut-off along the orbits, as calculated with the approximated formula in Section 1.4.2.

The average value is 11.26 GV, this can be used to obtain the primary proton spectrum using e.g. the local interstellar proton spectrum in [4].

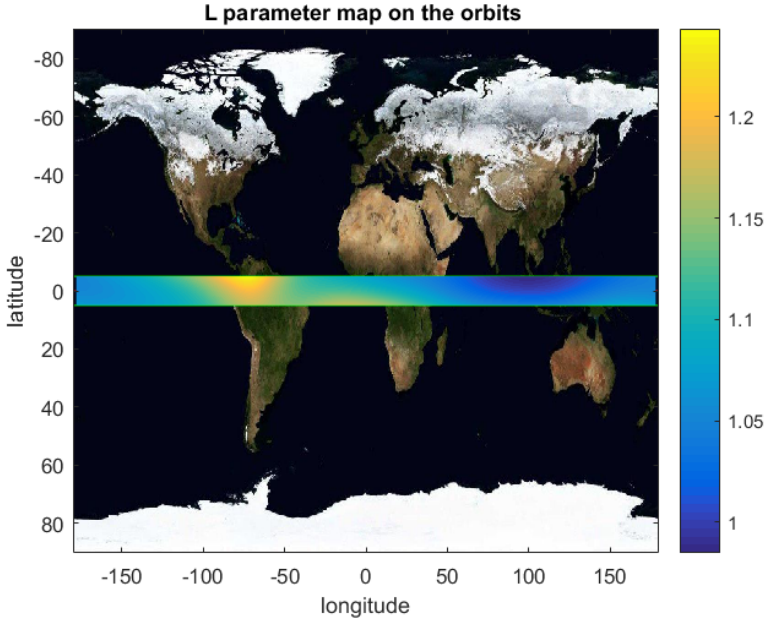

Figure 2.2: L value along the orbit

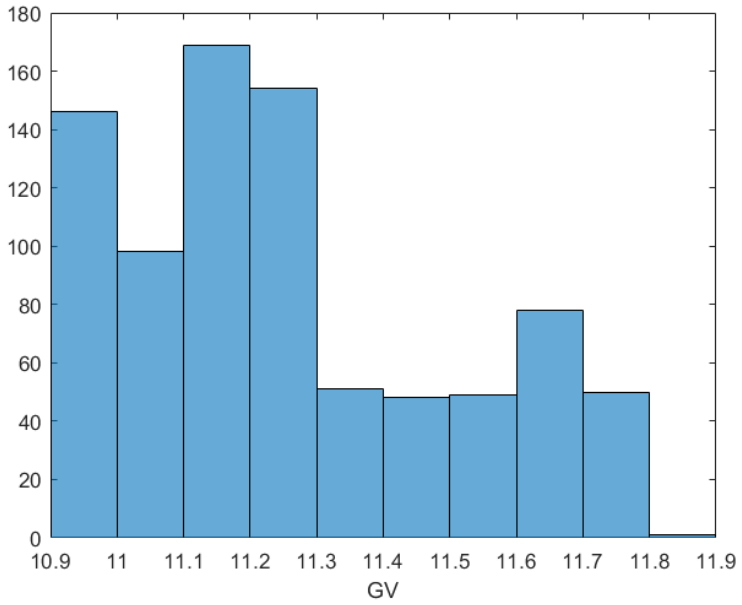

Figure 2.3: Time histogram of the geomagnetic cut-off rigidities along the orbit

2.3 Trapped Protons along the orbit

To obtain the proton fluxes along the orbit we use the AP9 model, from which we obtain a table of the trapped radiation that will reach the spacecraft as a function of coordinates and time. The model provide flux and cumulative fluence for several energy slots (from 0.1 to 2000 MeV).

From the AP9 program [8], using the orbit ephemerids as input, we obtain a file with the integral flux (from E=0.1 MeV to E=2000 MeV) for each 60 seconds time interval. We process this to calculate the the average flux for passages over the SAA and the average time of flight inside it using the differential flux at 1 MeV to track the contours of the SAA.

In Figure 2.4 we see the differential flux at 1 MeV as a function of the coordinates at 550 km, no limits on the other coordinates; the flux is non zero only in the SAA.

In Figure 2.5 we see the passages over the SAA characterized by peaks on the flux magnitude. Always in Figure 2.5 we see how orbit selects fluxes inside the SAA and how much the peak flux varies in the anomaly depending on how deep in we go (a factor 7). In Figure 2.6 we plotted the detail of the previous picture so we can see the shapes of the peaks.

In Figure 2.7 on top we show the possible value of 1 MeV proton fluxes as a function of longitude for our orbits, on bottom is represented the magnetic field to show how the flux overlap with the minimum of the magnetic field.

2.4 Transit in the SAA

Now we study how often our spacecraft will enter inside the SAA borders and how much time it passes inside and outside the anomaly. Since the orbit precedes around the Earth the time that the satellite spends inside the SAA varies. We define the SAA as the area where the 1 MeV flux is higher than 10 $\#/cm^2/s/MeV$, the zones where the fluxes are lower are outside.

Using the AP9 software we get the 1 MeV proton flux at every location along the orbit; the pattern is very similar to the one in Figure 2.6.
We mark down when the fluxes go under the 10 $\#/cm^2/s/MeV$ and we compute an

average flux of particles during the fly over the SAA.

In Figure 2.8 we have the results of this operation: in our two month simulation our spacecraft passes inside the SAA 844 times.
The average flux at 1 MeV is about $(180 \pm 3)\#/cm^2/s/MeV$. In Figure 2.9 we can better see the pattern of fluxes (detail of the first 10 days).

Another important information is the time of flight (Tof) through the SAA. We can find the Tof so that:

$$\Phi(1MeV) = \phi_{avg} \cdot Tof$$

Where:
ϕ_{avg} is the average 1 MeV flux in the SAA
Tof is the time of flight through the SAA
$\Phi(1MeV)$ is the 1 MeV total *fluence* of particles during the crossing of the SAA $[\#/cm^2/MeV]$

In our simulation are the maximum Tof is 25 minutes and the highest value of $\Phi(1MeV)$ is $4.44 \cdot 10^5\#/cm^2/MeV$.
The average crossing of the SAA is characterized by:

$Tof_{avg} \approx 16$ minutes
$\Phi_{avg}(1MeV) = (1.94 \pm 0.05) \cdot 10^5\#/cm^2/MeV$

In Figures 2.10 we plot the Tof and the $\Phi(1MeV)$ of all the crossings of the SAA and we obtain the flux of protons reaching the spacecraft.

We can see the periodicity on one day giving the ellipse shape and the long scale variation on top of it. In case a simple average value suffices, we plot also the average value that we calculated above as an asterisk.

In Figure 2.11 we show the time spent between two passages of the SAA, the average value is 84 minutes. The first plot is the trend of the whole simulation and the second one is the detail of the first 10 days of flight.

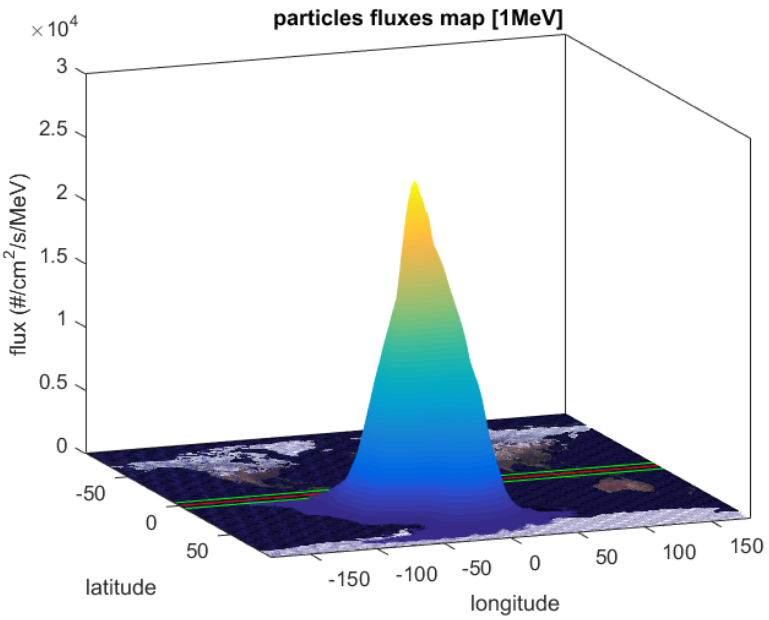

Figure 2.4: Differential Flux at 1 MeV as a function of latitude and longitude along our orbit in AP9 model

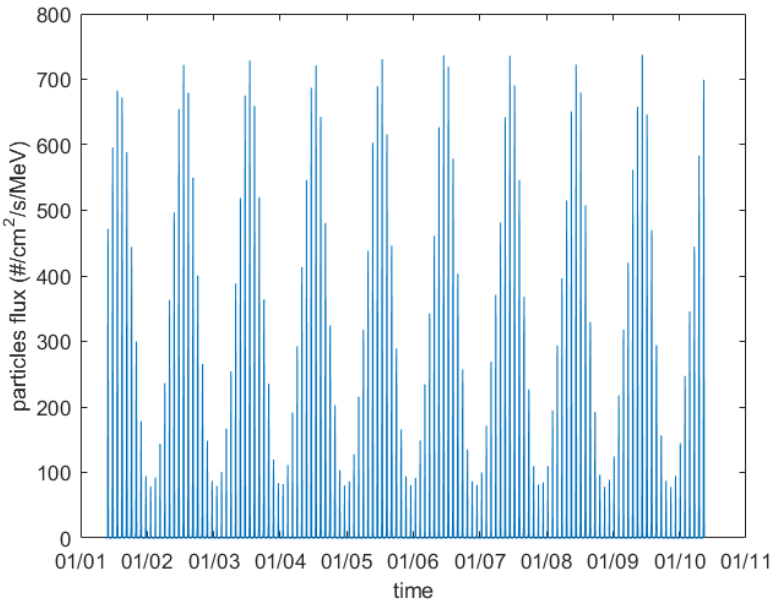

Figure 2.5: Differential flux at 1 MeV during 10 days

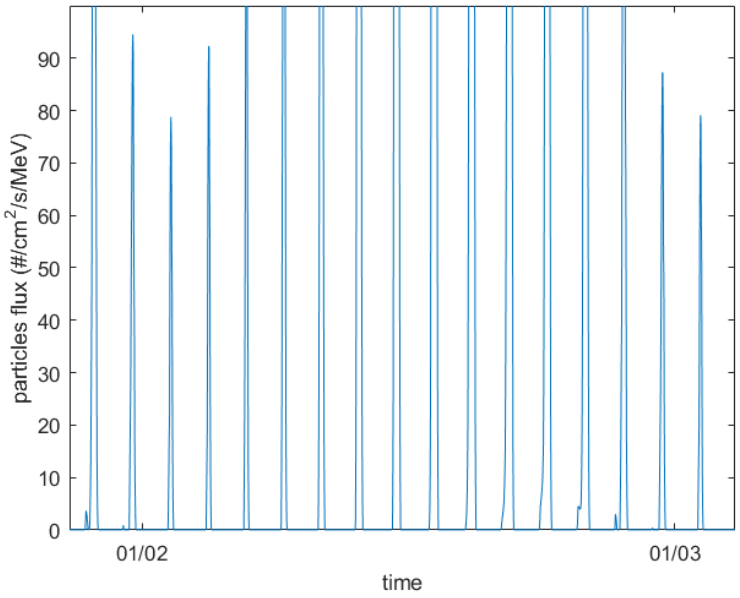

Figure 2.6: Detail of the daily flux variation

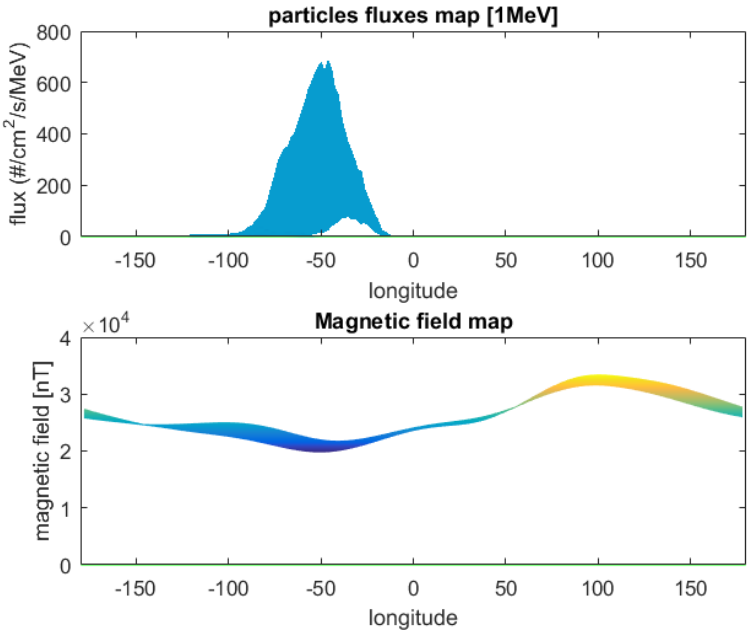

Figure 2.7: Comparison of the 1 MeV flux with the geomagnetic field intensity

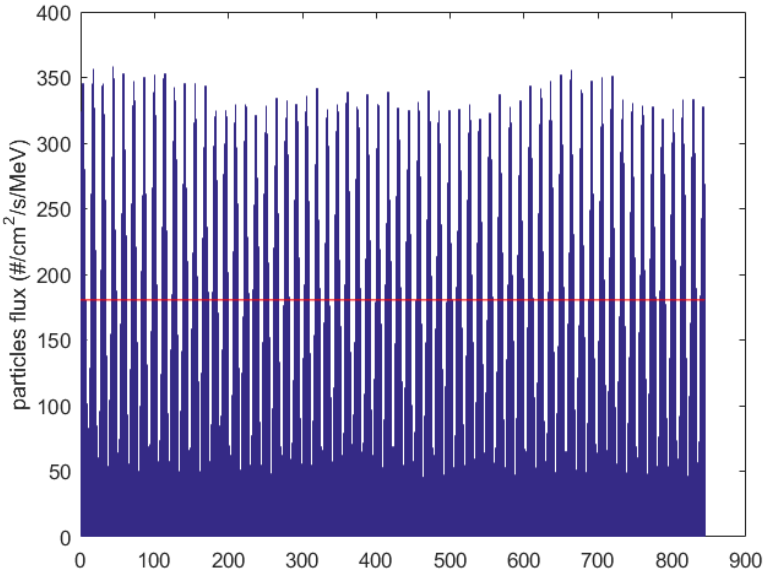

Figure 2.8: Average differential flux per passage in the SAA per orbit over the 2 month simulation; the red line is the mean value

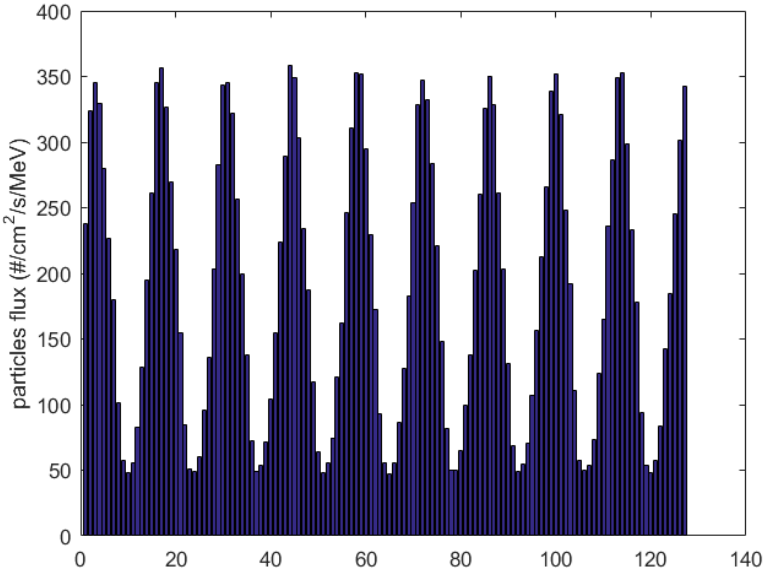

Figure 2.9: Same figure of 2.8 for 10 days

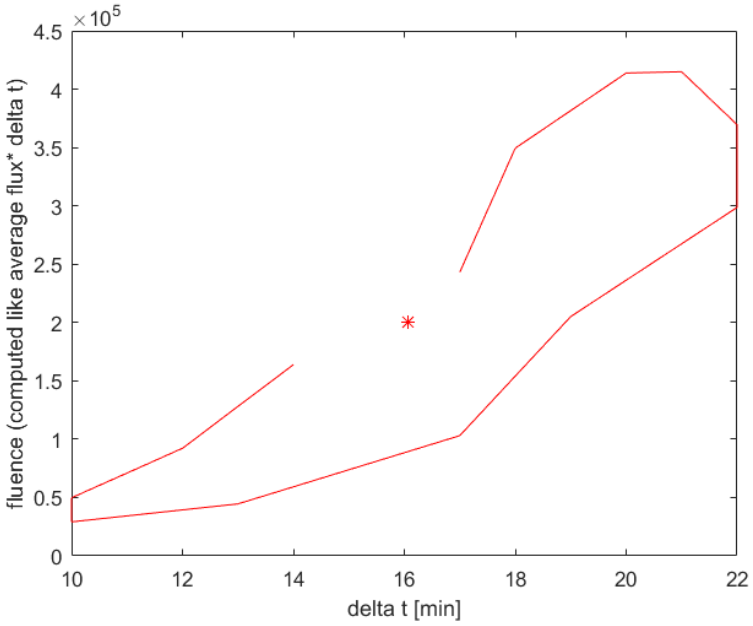
×10^5
4.5
4
3.5
3
2.5
2
1.5
1
0.5
0
10
12
14
16
18
20
22
fluence (computed like average flux* delta t)
delta t [min]

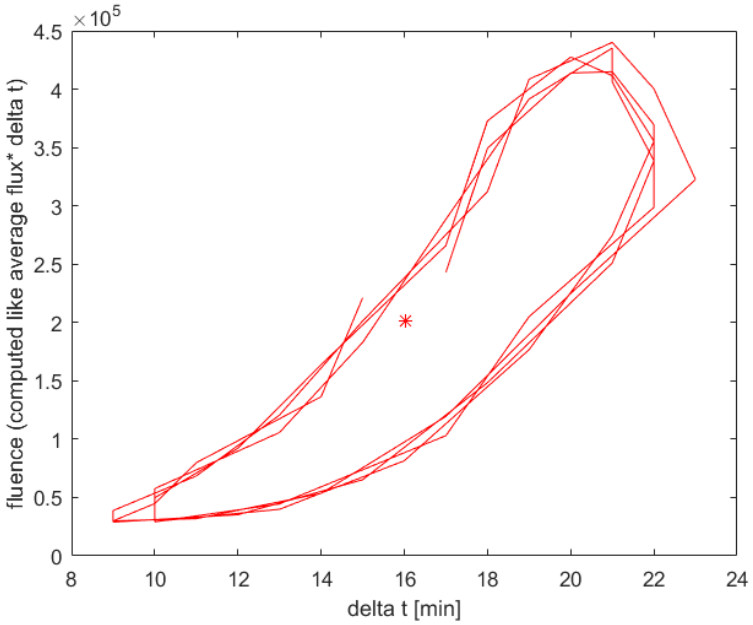
×10^5
4.5
4
3.5
3
2.5
2
1.5
1
0.5
0
8
10
12
14
16
18
20
22
24
fluence (computed like average flux* delta t)
delta t [min]

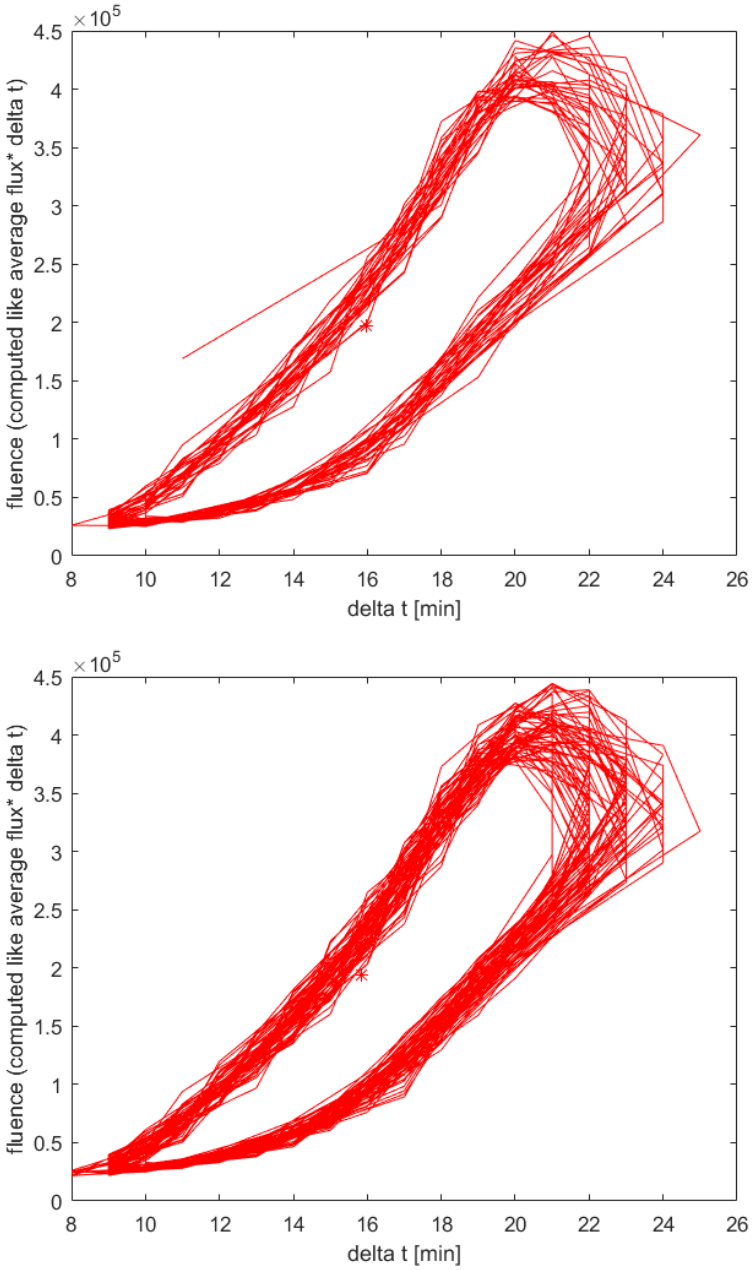

Figure 2.10: Φ versus Tof during (in order) 1,5,30,60 days. The * point is the average condition

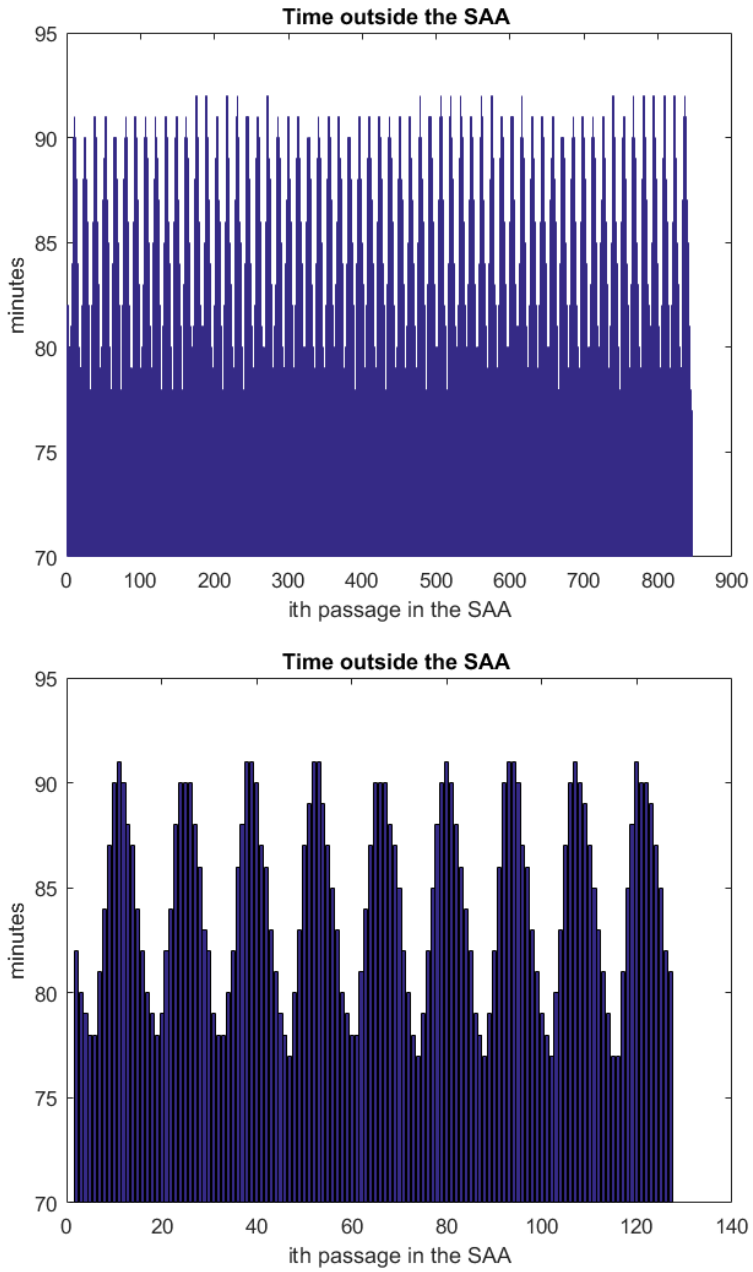

Figure 2.11: time outside the SAA during the simulation

2.5 Average irradiation profile

In the previous Section we used the differential flux at 1 MeV to derive the time inside the SAA inside and outside the SAA; this corresponds to an irradiation of 16 minutes followed by an OFF time of 84 minutes (in average). We can now use AP9 and derive the average differential spectrum in the ON phase.

In Figure 2.12 we show the average differential spectrum in the SAA from 100 keV to 1.2 GeV. In Table 2.1 we give the numerical values corrisponding to the plot.

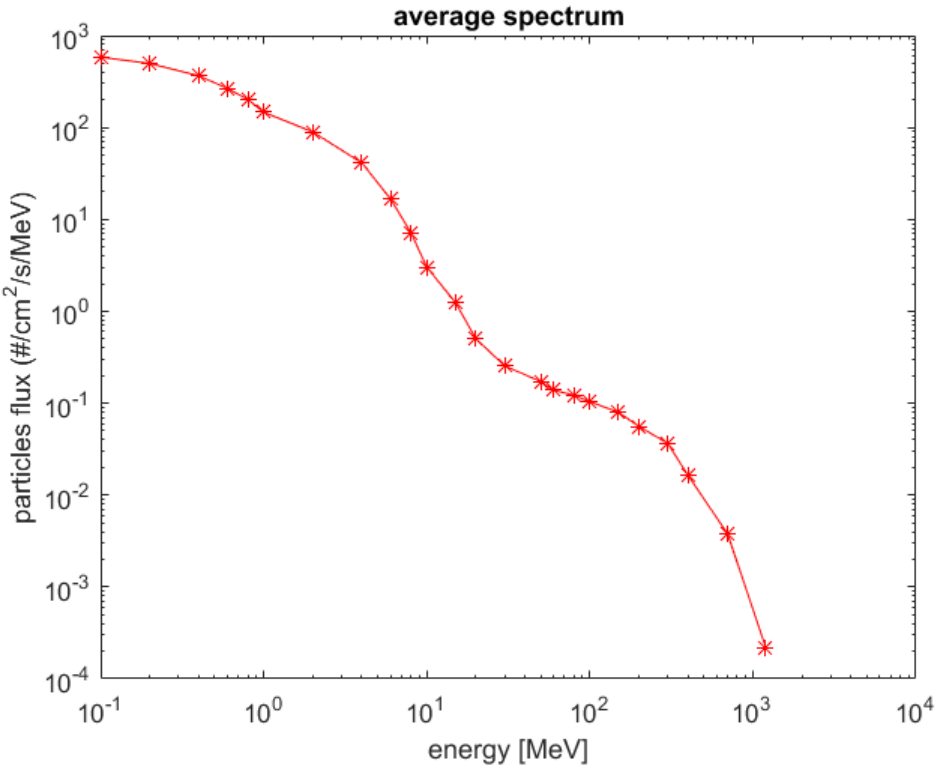

Figure 2.12: Average spectrum

In case the simple average is not enough but using the AP9 fluxes as function of time is to much of an hassle one can modulate this average flux with the plot in Figure 2.8.

Energy [MeV]	Average Flux $[\#/cm^2/s/MeV]$
0.1	607
0.2	519
0.4	381
0.6	277
0.8	210
1	152
2	93.1
4	43.1
6	17.7
8	7.71
10	3.28
15	1.36
20	0.551
30	0.279
50	0.188
60	0.151
80	0.133
100	0.113
150	0.0865
200	0.0606
300	0.0395
400	0.0175
700	0.00412
1200	0.000283
2000	/

Table 2.1: Average fluxes for every energy slot

Chapter 3

Out design conditions

The inclination we can expect depends strongly on the launch station and the available finances for orbit-plane maneuvers. To check an alternative orbit we study what happens for a 30 degrees inclination orbit, for an easy computation the simulation spaces about 30 days (For reference the Kennedy Space Center is at 28.4 degrees of latitude).

3.1 Flux in the SAA

With the 5 degrees inclined orbit we cross the anomaly in the upper zone where the particles fluxes are low.

As we expected, with the 30 degrees orbit we go deep into the SAA's core, and how we can see in Figure 3.1 the intensity of the fluxes increases by orders of magnitude. This increases the dangers for the microelectronic systems and the material activation.
From Figure 3.1 we can also observe that the SAA's border becomes larger especially towards the est direction.

3.2 Fluence profile

The higher inclination means more time spent in the SAA and higher fluence since we go deeper inside it where the magnetic field is lower.
In Figure 3.2 we plot the fluence versus the time passed inside the SAA for the 5 and 30 degrees. As we can see the maximum time of flight increase from 25 minutes to 35.

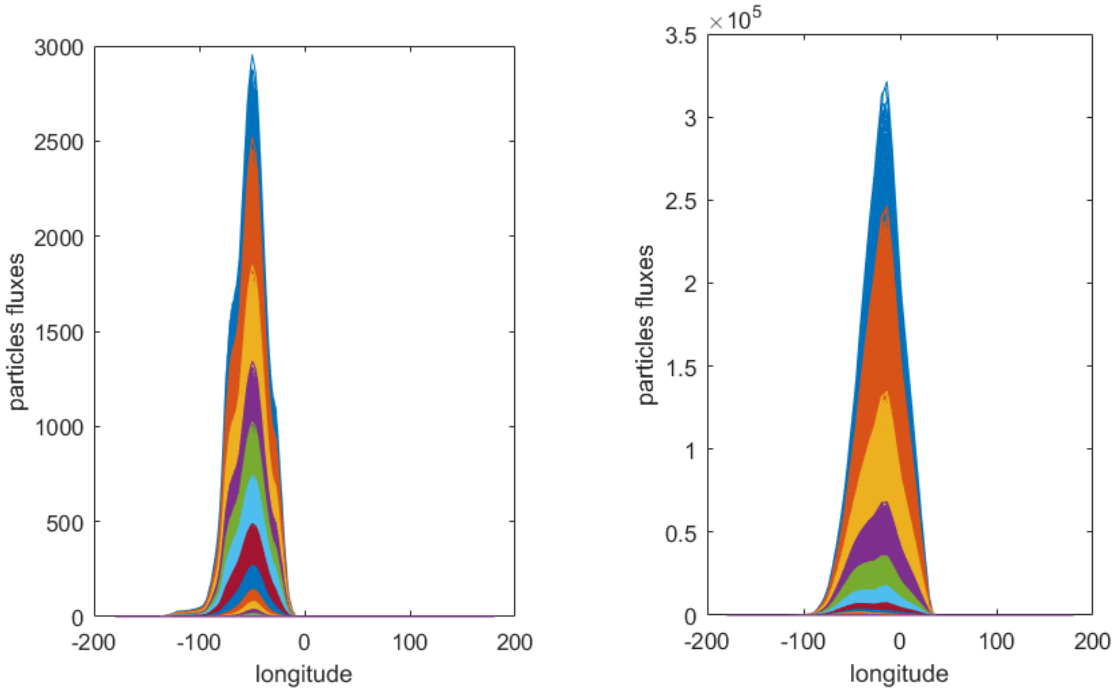

Figure 3.1: Flux as a function of the longitude and of energy (blue: 0.1 MeV, and other colors as in Table 2.1 for increasing energy

The 2D shape of the fluence becomes more complex than the low inclination one. In addition to the longer time of flight the average fluence inside the SAA increases by more than one order of magnitude. From the Figure 3.2 we have a max fluence that changes from Φ_{max} (1 MeV, 5 deg) $= 4.44 \cdot 10^5$ $\#/cm^2/MeV$ to the value of Φ_{max}(1 MeV, 30 deg)$= 1.40 \cdot 10^7$ $\#/cm^2/MeV$.

The average values of fluence and ON time become:

$Tof_{avg}(30deg) \approx$ 20 minutes
Φ_{avg}(1 MeV, 30 deg)$= (4.5 \pm 0.2) \cdot 10^6$ $\#/cm^2/MeV$.

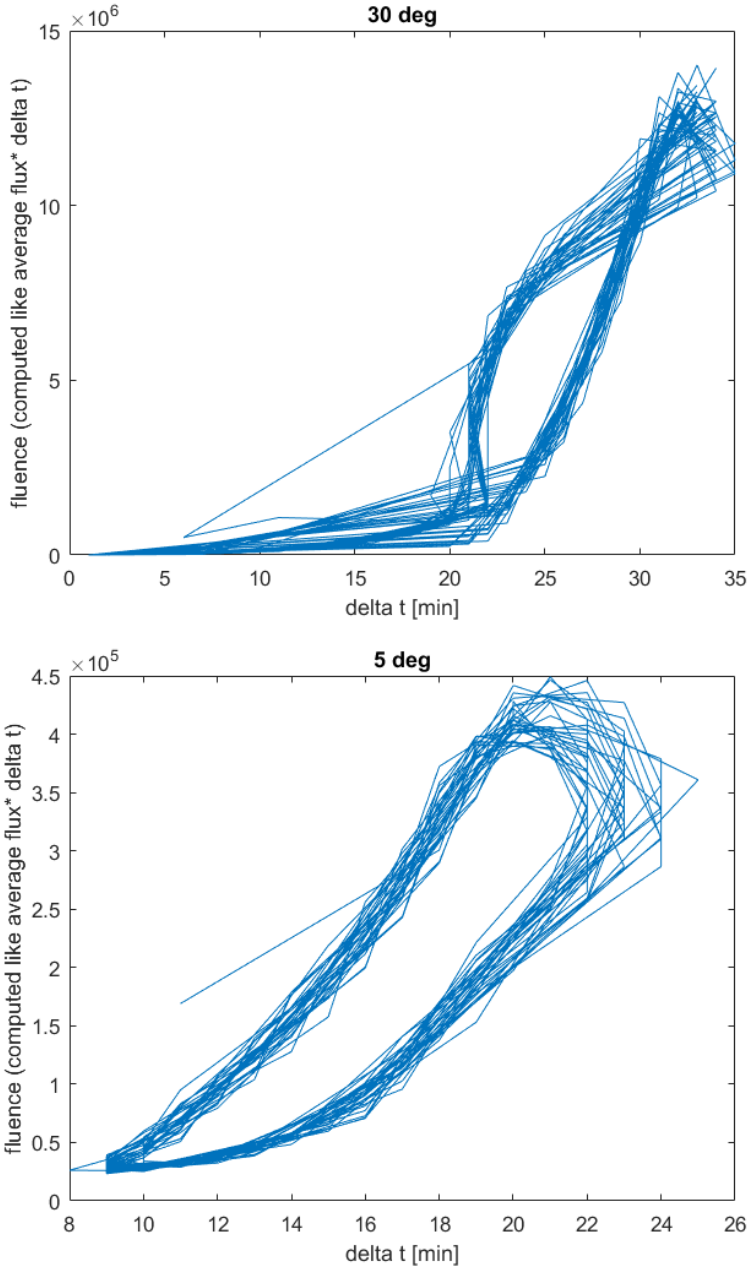

Figure 3.2: $\Phi(1MeV)$ versus Tof for the two inclination angle

Chapter 4

Conclusion

In this work we analyzed the proton irradiation profile due to trapped particles for a payload in a quasi-equatorial orbit in 550 km of altitude. The values that we obtained will be use to estimate radiation damage and material activation for a Compton Gamma Ray Space Telescope.

We also computed the rigidities cut-off to be applied to the spectrum of primary protons. We checked the impact of an higher inclination and as we expected the fluences become rapidly larger.

The next step in this work would be the computation of the neutron fluxes, which also cause material activation, and the dose caused by trapped electrons.

Bibliography

[1] Walt, Martin (1994), *Introduction to Geomagnetically Trapped Radiation*, Cambridge University Press , Cambridge.

[2] Thebault, Erwan (2015), *International Geomagnetic Reference Field: the 12th generation*, Earth, Planets and Space 2015.

[3] D.F Smart, M.A. Shea (2004), *A review of geomagnetic cutoff rigidities for earth-orbiting spacecraft*, Air Force Research Laboratory VSBX, Space Vehicles Directorate, 29 Randolph Road, Bedford, MA 01731, USA.

[4] C. Conti (2015), *Solar modulation of the proton local interstellar spectrum with AMS-02, VOYAGER 1 and PAMELA*, Physics and Astronomy Department, University of Hawaii at Manoa, Honolulu, HI 96822

[5] De Santis, Angelo (2008), *Are we going towards a global planetary magnetic change?* , Istituto Nazionale di Geofisica e Vulcanologia, Sezione di Roma 2 Via di Vigna Murata 605, 00143 Roma, ITALY

[6] *Vette, J. I., The NASA/National Space Science Data Center Trapped Radiation Environment Model Program (1964-1991), NSSDC/WDC-A-R&S 91-29*,1991b.

[7] Andreetta, Sara (2017), *Study of material activation in nanosatellites for gamma-ray astrophysics (ID Code 56942)*, Università degli studi di Padova, Padova, bachelor thesis.

[8] *https://lws-set.gsfc.nasa.gov/documents/AE9AP9_overview14Jun2012.pdf*

Appendix

4.1 Software used in this thesis

All the computation was done in Matlab. I used "International Geomagnetic Reference Field (IGRF) Model" (by Drew Compston) for the conversion of coordinates and the "IGRF Magnetic Field" (by Kip Knight) to compute the L parameters. All the packages that I have used in this thesis were taken from Mathworks.com

I used the AP9/AE9 software suite for the computation of the spacecraft ephemerids and for the proton fluxes.